Received: November 14, 2022. Revised: December 13, 2022.

International Journal of
Intelligent Engineering & Systems

http://www.inass.org/

Prediction of the Performance of Photovoltaic Modules from the Behavior of Physical Parameters According to Irradiance and Temperature

Bouchaib Zohal[1] Houssam Amiry[1] Said Yadir[2] Elhadi Baghaz[1]*
Rachid Bendaoud[1] Abderrahim El-Abidi[2] Fatima Chanaa[1] Mohammadi Benhmida[1]

[1]*Laboratory of Electronics, Instrumentation and Energy, Faculty of Science, Chouaib Doukkali University, El Jadida, Morocco.*
[2] *Laboratory of Materials, Processes, Environment and Quality, National School of Applied Sciences, Cadi Ayyad University, Safi, Morocco.*
* Corresponding author's Email: s.yadir@uca.ma

Abstract: In this paper, a study on photovoltaic module physical parameters behavior depending on irradiance *G* and module temperature T_M is presented. From this investigation, new equations translating physical parameters behavior depending on T_M and G are developed. The new proposed laws, which combine the effects of *G* and T_M in a correlated manner, have the advantage of incorporating G effect on the temperature coefficients by including specific terms. The developed laws form a basis for predicting PV module performance and can be incorporated into maximum power point tracking (MPPT) programs to extract peak power output under different operating conditions. This study is conducted by examining the electrical performances at the maximum power (I_m, V_m), the open circuit (0, V_{OC}), and the short circuit (I_{SC}, 0) points measured using an elaborate experimental platform. The photovoltaic module used is a monocrystalline type exposed to four G values of 700, 800, 880 and 1000 W.m^{-2} for temperatures T_M between 16°C and 48°C.

Keywords: PV modules performance, Physical parameters behavior, Temperature and irradiance effects, Performance prediction, I-V curve tracer.

1. Introduction

The most elementary equivalent electrical circuit of a photovoltaic (PV) cell (Fig. 1), which corresponds to single diode model (SDM), includes an ideal diode with a saturation current (I_0) and an ideality factor (n), a current generator delivering a photo-current of intensity I_{ph}, and a series (R_S) and a shunt (R_{SH}) resistances [1].

The SDM model's equation (Fig. 1) is given by :

$$I(V) = I_0\left(\exp\left(\frac{V-R_S I}{n V_{th}}\right)-1\right)+\frac{V-R_S I}{R_{SH}}-I_{ph} \quad (1)$$

I_0, I_{ph}, R_S, R_{SH}, and n represent the five physical parameters. $V_{th} = k_B T_M/e$, with k_B: Boltzmann constant, T_M: PV cell temperature, e: elementary charge.

Photovoltaic cell characterization consists of experimental current-voltage (I-V) measurements, extracting the physical parameters model and analyzing them to understand its electrical properties and identify loss mechanisms. Extraction and evolution study of the PV cells physical parameters under different climatic conditions can be useful to improve their efficiency.

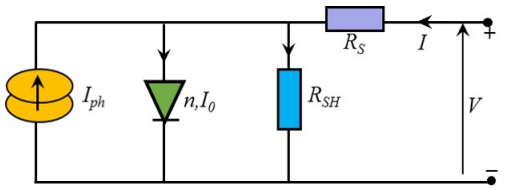

Figure. 1 PV cell SMD model

Many research studies have investigated the effect of changes in irradiation (G) and PV module temperature (T_M) on their performance and physical parameters. I0 parameter is considered in some work

to be independent of the irradiance level [2]. Further studies have found decrease in I_0 with G [3]. In contrast to these found results, studies have shown that I_0 grows with irradiance [4]. I_0, resulting from minority carriers generated thermally, is quite sensitive to temperature variation. Some work has found that I_0 undergoes an exponential increase with T_M [3]. Khan et al. [5] have found that I_0 has an inverse behavior with T_M.

The R_S parameter, related to the resistive losses in the different PV cell constituents, has an important effect on the electrical performance. In the literature three behaviors of R_S as a function of G have been observed. R_S can decrease [5], increase [6] or be independent with G [4]. Furthermore, two behaviors of R_S as a function of T_M have been generally observed. R_S can increase linearly [7] or decrease [3] with rising temperature.

Ideality factor (n) value depends on the type and quality of the used materials, the type of used junction and the solar cell manufacturing processes [7]. By considering the SDM model, n is assumed as independent of T_M and G [1]. In several studies, the results obtained show that when irradiance increase, n decreases if G is below 300 W/m^2 and increases if G is above 300 W/m^2 [6]. Fébba et al [8] have found that n undergoes a small linear decrease for G ranging from 600 W/m^2 to 1000 W/m^2. T_M influence on n has also been investigated in several studies. Singh et al [9] noted that n is independent of T_M, however, Bendaoud et al [2] showed that n decreases linearly with increasing temperature.

Shunt resistance (R_{SH}) has a slight effect on solar cell efficiency [2]. Several studies found that R_{SH} increases with G [1] and others have shown an opposite behavior G [3]. T_M effect analysis on the physical parameters in some works shows a linear decrease of R_{SH} [9]. Photogenerated current (I_{ph}) behavior shows a perfectly linear increase with T_M and G [8].

The prediction of the performance of PV system installations under real operating conditions has been the subject of several studies [10]–[14]. Studies have proposed empirical laws expressing the variation of PV module performances, such as maximum power (P_{max}), V_{OC}, I_{CC} and conversion efficiency, as a function of T_M and G [10]. Other works introduce correction coefficients into these laws that take into account the effects of other factors on PV module performance, among which are incidence angle and solar spectral distribution [15]. Besides these studies, some work has been carried out to predict the performances according to the climatic conditions based on the physical parameter's extraction. This approach has the advantage of providing more information than the first one and of reconstructing the whole I-V characteristics. However, the laws variation depending on G and T are proposed for only a some physical parameters and the performances are deduced by considering some approximations [16].

In this work, the impact of T_M and G on the physical parameters of PV modules is evaluated. For this purpose, the physical parameters extraction is carried out by exploiting the experimental data corresponding to the points (V_m, I_m), (V_{OC}, I=0), and (V=0, I_{SC}), measured under actual operating environment by a high-resolution characterization platform [1]. Based on the findings of the physical parameter's behavior, new equations translating the T_M and G influences are developed. The reliability of the developed equations is evaluated by comparison with those reported in the scientific literature. The developed equations can serve as bases to predict the *I-V* characteristics and to locate the maximum power point under changing climatic conditions. After introduction, this work is organized as follows: Section 2 outlines the extraction method used. Section 3 presents the experimental data used and their equivalent equations obtained by regression. Section 4, results and discussion, presents the physical parameters extraction results, the corresponding equations modeling their behavior as a function of T_M and G, and comparison results with other scientific literature models. The conclusion of this work, outlines the main points and presents perspectives.

2. Extracting physical parameters

Extraction of I_0, I_{ph}, R_S, R_{SH}, and n parameters, in the SDM framework, is achieved by solving a five-equation system deduced from Eq. (1) [4]. Three equations are obtained by writing equation (1) at (V_m, I_m), (V_{OC}, I=0), and (V=0, I_{SC}) points of the I-V characteristic (Fig. 2). Two other equations are obtained by deriving Eq. (1) with respect to V at the points (I_{SC}, 0) and (V_{OC},0). The system of these five equations can be deduced and solved using a Newton-Raphson algorithm.

By combining three equations, the system becomes a set of four equations depending on R_S, R_{SH}, I_0 and n :

$$I_0\left(\exp\left(\frac{V_{OC}}{n\,V_{th}}\right)-\exp\left(\frac{-R_S I_{SC}}{n\,V_{th}}\right)\right)+\frac{V_{OC}}{R_{SH}}+ I_{SC}\left(1+\frac{R_S I_{SC}}{R_{SH}}\right)=0 \quad (2)$$

$$(R_{S0}-R_S)\left(\frac{1}{R_{SH}}+\frac{I_0}{n\,V_{th}}\exp\left(\frac{V_{OC}}{n\,V_{th}}\right)\right)-1=0 \quad (3)$$

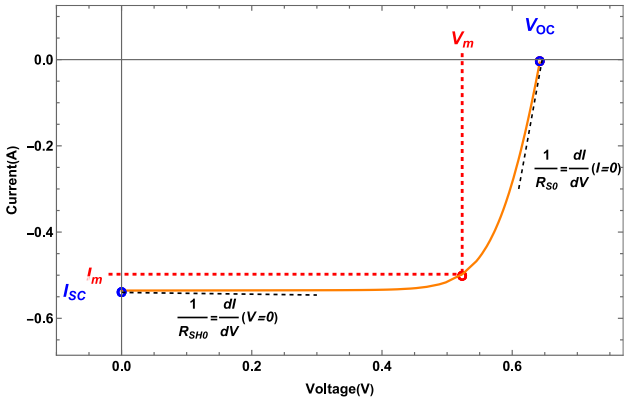

Figure. 2 *I-V* characteristic of an illuminated photovoltaic cell

Table 1. Manufacturer's specifications of the used PV module under STC conditions

Technical specifications	
Module	410M
Cell type	m-Si
Maximum power point (P_{max})	10 W
Maximum power current (I_m)	0.59 A
Maximum power voltage (V_m)	16.8 V
Current I_{SC}	0.65 A
Voltage V_{OC}	21 V
I_{SC} Temperature coefficient (%/°C)	0.01
V_{OC} Temperature coefficient ((%/°C)	-0.36

$$(R_{SH0}-R_S)\left(\frac{1}{R_{SH}}+\frac{I_0}{n\,V_{th}}\exp\left(\frac{-R_S I_{CC}}{n\,V_{th}}\right)\right)-1=0 \quad (4)$$

$$I_0\left(\exp\left(\frac{V_{OC}}{n\,V_{th}}\right)-\exp\left(\frac{V_m-R_S I_m}{n\,V_{th}}\right)\right)+\frac{V_{OC}-V_m}{R_{SH}}+ I_m\left(1+\frac{R_S I_m}{R_{SH}}\right)=0 \quad (5)$$

3. Characterization of PV generator in real operating conditions

Table 1 shows some technical parameters of the photovoltaic generator (PVG) studied, which is composed of N_S = 36 cells connected in series.

3.1 Experimental platform for data acquisition in real operating conditions

Typically, PV generator characterization is achieved in a laboratory setting using solar simulators. The main advantage is that the factors affecting the measurements can be controlled. Measuring devices and solar simulators are manufactured to operate under conditions close to STC conditions. However, the spectral compositions of the radiation emitted by solar simulators are significantly different from that of sun light. Characterization under real operating conditions provides several advantages over laboratory characterization. The incident light in this case is on a clear weather and extremely uniform over the entire surface of the module regardless of its size. In addition, it provides all the illumination, temperature and incidence conditions necessary for the characterization of a PV generator. However, this solution has some drawbacks, such as the continuously varying weather conditions. Proper instrumentation, however, is required to measure all experimental data. Fig. 3 shows the experimental platform [1] used to collect, under real operating conditions, each single *I-V* characteristic at constant T_M and G.

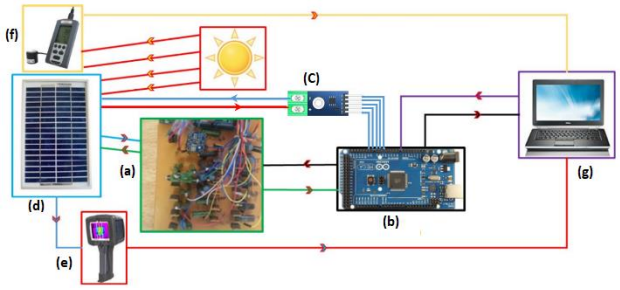

Figure. 3 Experimental platform composed of (a and b) data acquisition system, (c) Temperature sensor, (d) Photovoltaic module, (e) Thermal camera, (f) Solarimeter, and (g) Computer

3.2 Experimental data and their equivalent regression equations

Owing to the uncertainty of the measurements, the experimental data collected at the points (*I*, *V*) considered may show some fluctuations and dispersions. In order to ensure optimal results, regression equations, derived from the literature (Table 2), are established to characterize the evolutionary trend of the experimental data at the three considered *I-V* points with respect to T_M and G. Using this regression equations, the parameters evolution can be determined more reliably. Fig. 4 shows the evolution of V_{OC}, I_{SC}, I_m, V_m, R_{S0}, and R_{SH0} as a function of temperature obtained using equations reflecting the trend of experimental data of a monocrystalline module carried out under real operating conditions.

4. Results and discussion

4.1 Physical parameters extraction results

Fig. 6 illustrates the experimental characteristics and the extracted ones using the regression equations for T_M between 16 °C and 48 °C and four irradiation levels. The different characteristics presented in this

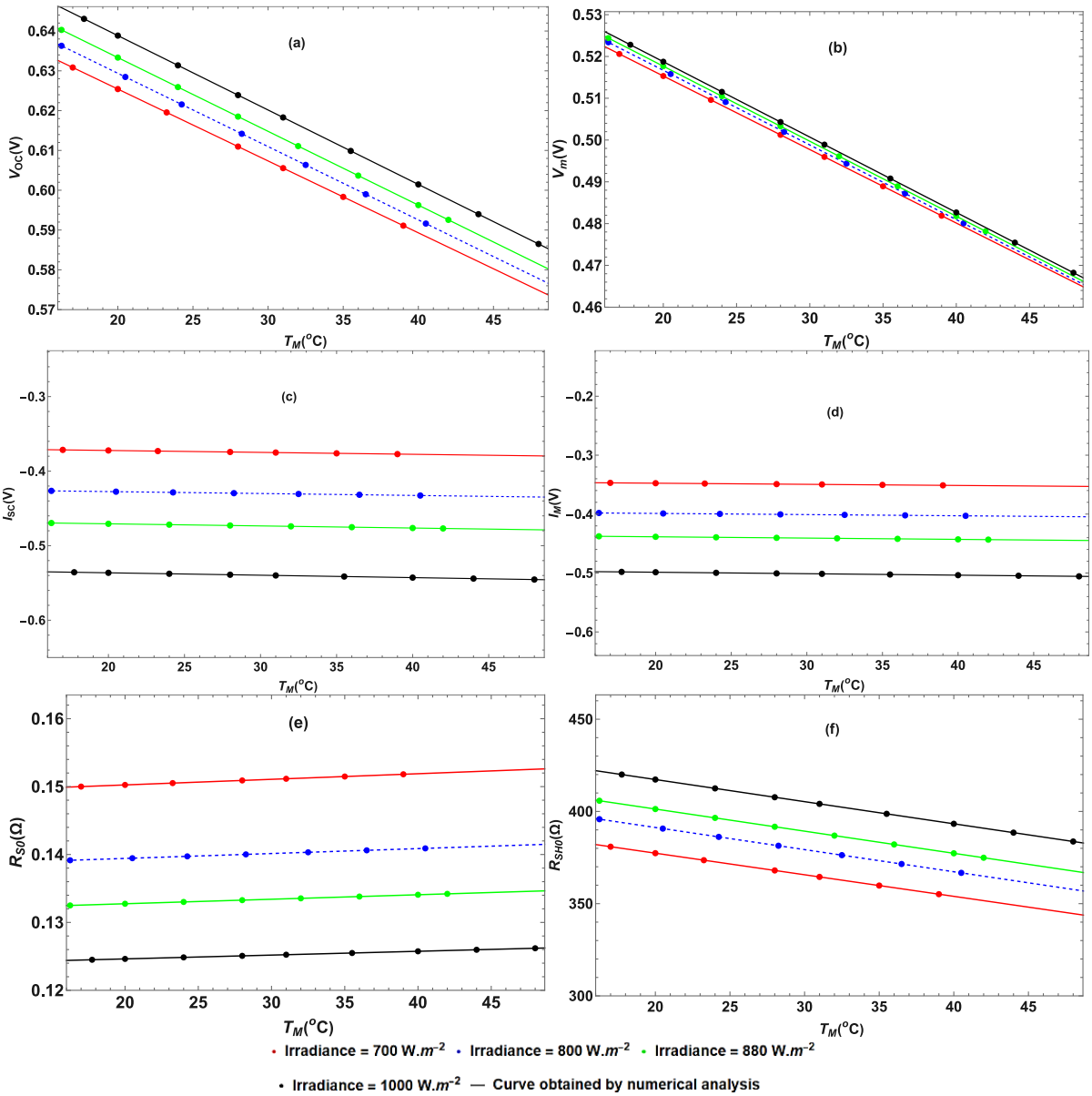

Figure. 4 PV module's performance as function as T_M: (a) V_{OC}, (b) V_M, (c) I_{SC}, (d) I_M, (e) R_{S0}, and (f) R_{SH0}

Table 2. PV module performance equations depending on T_M and G

Correlation equation	Coefficients values
$V_{OC} = V_{OC,ref}\left(1-\alpha_1\left(T_M - T_{M,ref}\right)\right) \times \left(1+\beta_1\, Ln\left(G/G_{ref,T_0}\right)\right)$ (6)	$V_{OC,ref}$ = 0.6295 V $\alpha_1 \approx$ 0. 00297/°C and $\beta_1 \approx$ 0. 0634
$V_m = V_{m,ref}\left(1-\alpha_2\left(T_M - T_{M,ref}\right)\right) \times \left(1+\beta_2\, Ln\left(G/G_{ref,T_0}\right)\right)$ (7)	$V_{m,ref}$ = 0.6295 V $\alpha_2 \approx$ 0. 00352/°C and $\beta_2 \approx$ 0. 0177
$I_{SC} = I_{SC,ref}\left(1+\alpha_3\left(T_M - T_{M,ref}\right)\right) \times \left(G/G_{ref,T_0}\right)$ (8)	$I_{SC,ref}$ = - 0. 5380 A and α_3= 0.0006/ °C
$I_m = I_{m,ref}\left(1+\alpha_4\left(T_M - T_{M,ref}\right)\right) \times \left(G/G_{ref,T_0}\right)$ (9)	$I_{m,,ref}$ = - 0.4999 A and $\alpha_4 \approx$ 0.0005 /°C
$R_{S0} = R_{S0,ref}\left(1+\alpha_5\left(T_M - T_{M,ref}\right)\right) \times \left(G_{ref,T_0}/G\right)^{\beta_5}$ (10)	$R_{S0,ref}$ = 0. 1250V $\alpha_5 \approx$ 0. 000495/°C and $\beta_5 \approx$ 0. 5172
$R_{SH0} = R_{SH0,ref}\left(1+\alpha_6\left(T_M - T_{M,ref}\right)\right) \times \left(G_{ref,T_0}/G\right)^{-\beta_6}$ (11)	$R_{SH0,ref}$ = 411.3 V $\alpha_6 \approx$ 0. 00305/°C and $\beta_6 \approx$ 0. 2906

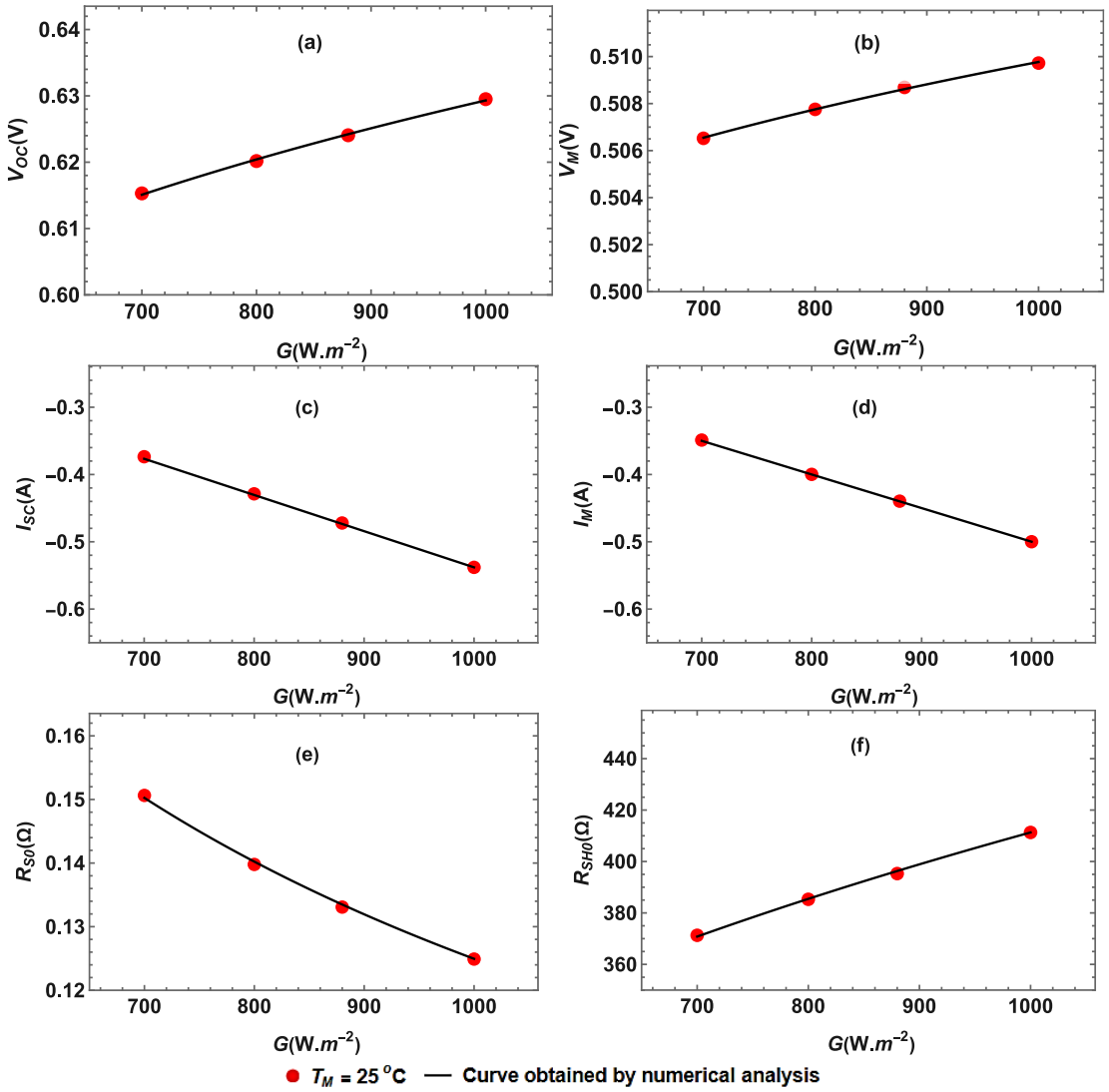

Figure. 5 Variation of the PV module's performance with respect to G: (a) V_{OC}, (b) V_M, (c) I_{SC}, (d) I_M, (e) R_{S0}, and (f) R_{SH0}

figure testify to good agreement of experimental PV cell characteristics with those predicted by extraction.

4.2 Statistical evaluation

Three statistical indicators are used to assess the accuracy of the extraction (Table 3) [1], [17] :

- The mean absolute relative error (*MARE*): is sensitive to extreme and low values. *MARE* gives an idea of the prediction quality in relation to the measured greatness values.
- The coefficient of determination (R^2): stands for the fraction of predicted data that is close to those measured. The coefficient of determination is a number between 0 and 1. The closer the R^2 is to 1, the closer the scatterplot obtained by extraction is to the experimental one.
- *erMax*: is the maximum value of absolute relative errors. Thus, lower its value, better is the predictive capacity of a extraction method.

Table 3. Statistical indicators used to evaluate the extraction method

Indicator	Ideal value	Equation
MARE	0	$MARE = \frac{1}{p}\sum_{i=1}^{p}\left\|\frac{I_{m_i} - I_{C_i}}{I_{m_i}}\right\|$
R^2	1	$R^2 = 1 - \frac{\sum_{i=1}^{p}(I_{m_i} - I_{C_i})^2}{\sum_{i=1}^{p}(I_{m_i} - I_{avg})^2}$
erMax	0	$erMax = Max(\lvert I_{m_i} - I_{C_i}\rvert)$

In Table 4, the results obtained using the three statistical indicators equations are presented. The results show a quite satisfactory compatibility between the experimental measurements and the extraction results for different temperature and irradiance values, as might be expected from the

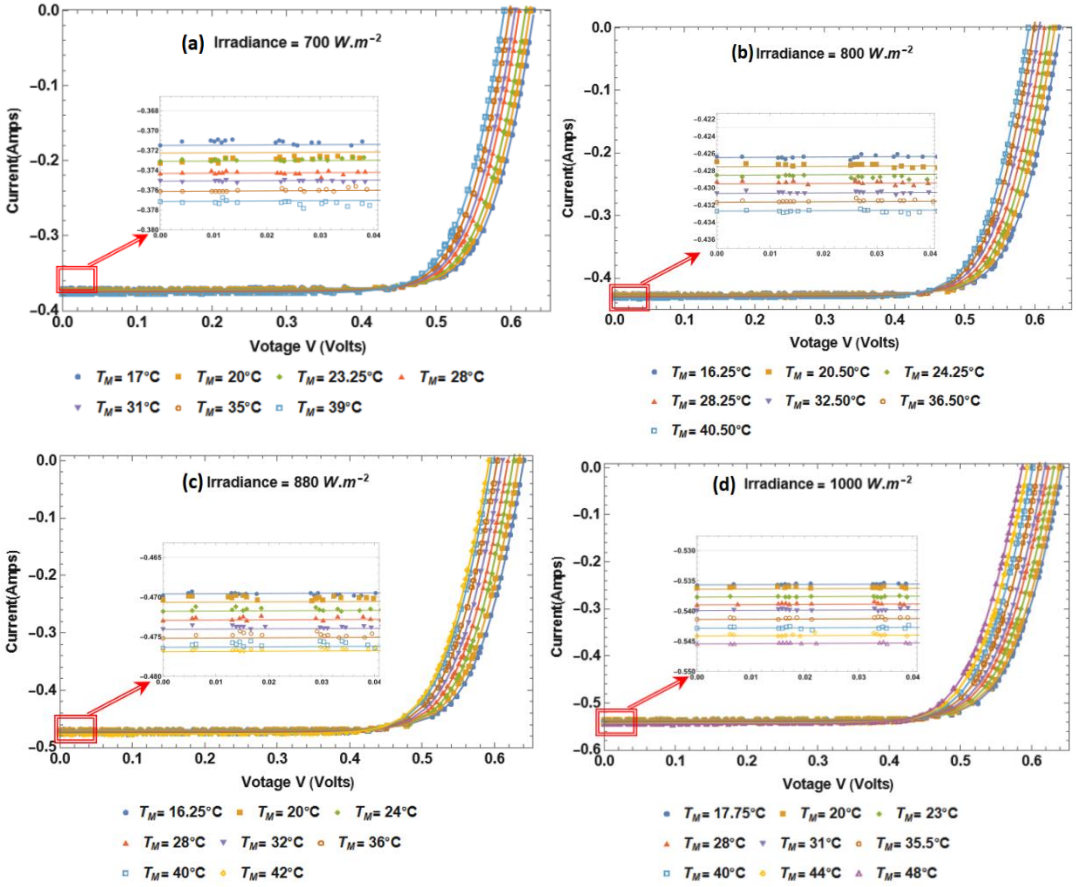

Figure. 6 Experimental *I-V* characteristics (•) and those obtained from extracted physical parameters (−) for different values of T_M and G

Table 4. Statistical evaluation of the of the characteristics generated using the extracted parameters

G (W.m^{-2})	T_M (ºC)	*MARE*	R^2	*erMax (A)*
700	17	0.0060	0.9994	0.5638
	20	0.0081	0.9995	0.2772
	23.25	0.0114	**0.9991**	0.5470
	28	0.0124	0.9990	0.4370
	31	0.0103	0.9992	0.9301
	35	0.0107	**0.9991**	0.2378
	39	0.0077	0.9995	**1.1458**
800	16.25	0.0047	0.9998	0.0058
	20.5	0.0043	0.9998	0.0038
	24.25	0.0031	**0.9999**	0.0029
	28.25	0.0042	0.9998	0.0065
	32.5	0.0058	0.9998	0.0055
	36.5	0.0042	0.9997	0.0069
	40	0.0051	0.9998	0.0037
880	16.25	0.0041	0.9998	0.0057
	20	**0.0168**	0.9998	0.0094
	24	0.0132	0.9997	0.0113
	28	0.0052	0.9998	0.0057
	32	0.0042	0.9998	0.0066
	36	0.0052	0.9998	0.0061
	40	**0.0028**	**0.9999**	0.0069
	42	0.0057	0.9997	0.0077
1000	17.75	0.0152	0.9998	0.0073
	20	0.0072	0.9998	0.0073
	24	0.0063	0.9997	0.0046
	28	0.0042	**0.9999**	**0.0004**
	31	0.0097	0.9996	0.0179
	35.5	0.0069	0.9997	0.0105
	40	0.0098	0.9996	0.0141
	44	0.0061	0.9997	0.0094
	48	0.0052	**0.9999**	0.0062

characteristic curves in Fig. 6. This highlights the accuracy and reliability of the extraction results.

4.3 Physical parameters behaviors depending on T_M and G

The injection of calculated values from the regression Eq. (6), Eq. (7), Eq. (8), Eq. (9), Eq. (10), and Eq. (11), in Eq. (2), Eq. (3), Eq. (4), and Eq. (5), allows to extract I_0, I_{ph}, R_S, R_{SH}, and n for different T_M and G values. Fig. 7 shows the evolution of R_S, n, I_0, R_{sh} and I_{ph} depending on T_M for four G values.

Fig. 8 shows the variations of the extracted

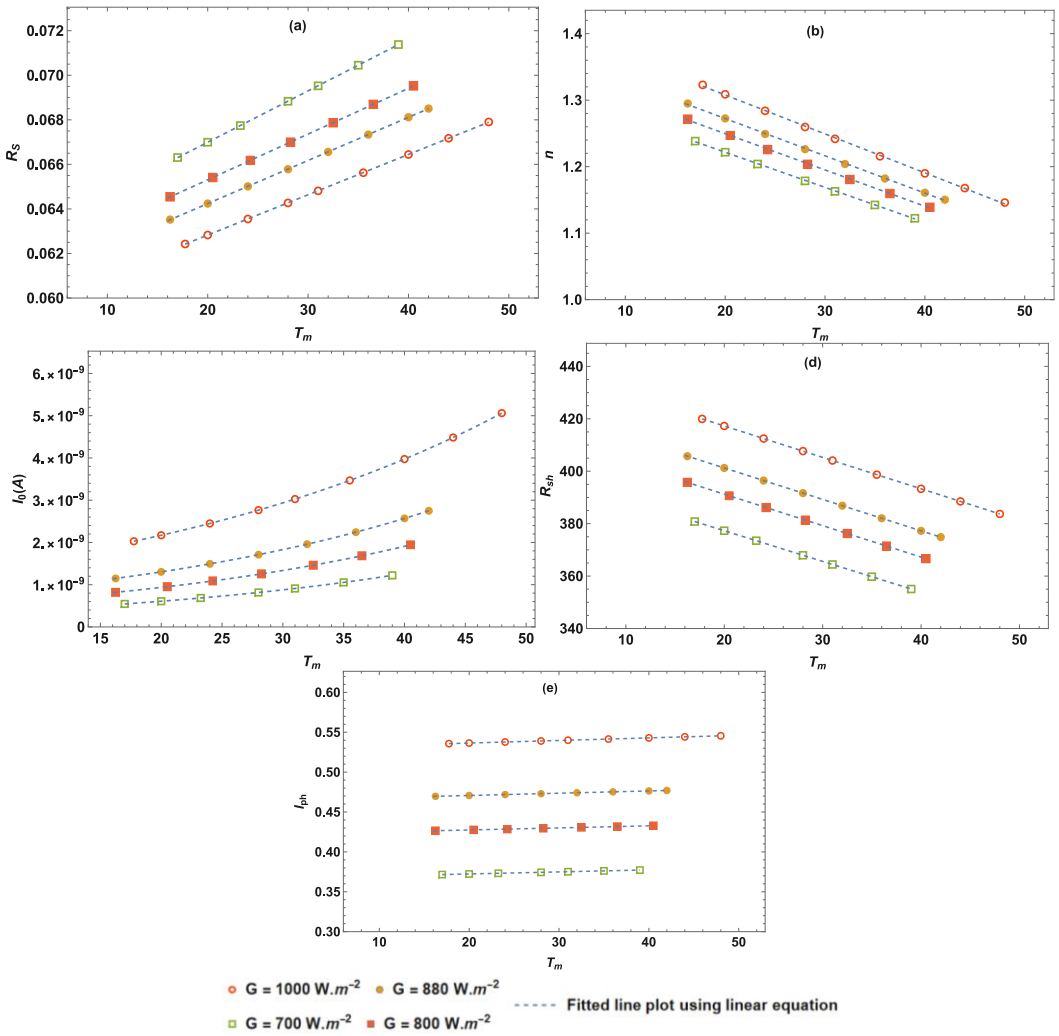

Figure. 7 PVG physical parameters evolution depending on T_M and G :(a) R_S; (b) n; (c) $R_{SH;}$ (d) I_0; (e) I_{ph}.

physical parameters (R_S, n, $R_{SH,}$ I_0, I_{ph}) depending on irradiance for T_M = 25 °C.

To investigate the irradiance impact on the temperature coefficients representing the slopes of the curves shown in Fig. 8, we plotted their variations as a function of G (Fig. 9).

For each irradiance value, the series resistance R_S undergoes a linear increase with $\boldsymbol{T_M}$. This behavior can be attributed to the rise in the predominant resistance values of metal grid and emitter sheet [1], [2] and owing to the reduced mobility in the PV cell material [18]. The ideality factor n shows a behavior opposite to that of R_S with T_M. The value of n provides information on the type of mechanism involved in the charge carriers transport across the p-n junction [19]. The transport process is purely of diffusion if n = 1 and mainly of recombination if n tends to 2 [7]. The results obtained show that n decreases towards 1 as T_M increases, improving the minority carrier diffusion process by decreasing the semiconductor active layer resistance or the temperature effect on the Shockley Read Hall and surface recombination mechanisms [1]. R_{SH} behavior shows a linear decrease with temperature (Fig. 7 (d)). This mechanisms [1]. R_{SH} behavior shows a linear decrease with temperature (Fig. 7 (d)). This decrease is attributed to the simultaneous influence of carriers trapping/untrapping and tunneling across levels of localized defects in semiconductors causing a current leakage through the p-n junction [2]. I_0 undergoes exponentially increase with increasing temperature as shown in Fig. 7 (c). I_0 provides an information on the recombination in the neutral regions. The value of I_0 reflects the rate of carrier leakage or recombination . Its increase due to the additional thermal activation of carriers [1]. Fig. 7 (e) shows a slight I_{ph} increase with T_M. Indeed, the band gap shrinks by increasing temperature and allows for the absorption of more photons, thus producing more charge carriers [1].

The increase of n and I_0 is a result of the recombination current increase (Fig. 7 (b) and (c)) [4]. Indeed, as G increases the photovoltaic effect generates more free charge carriers. This increases the probability of charge carries recombination and

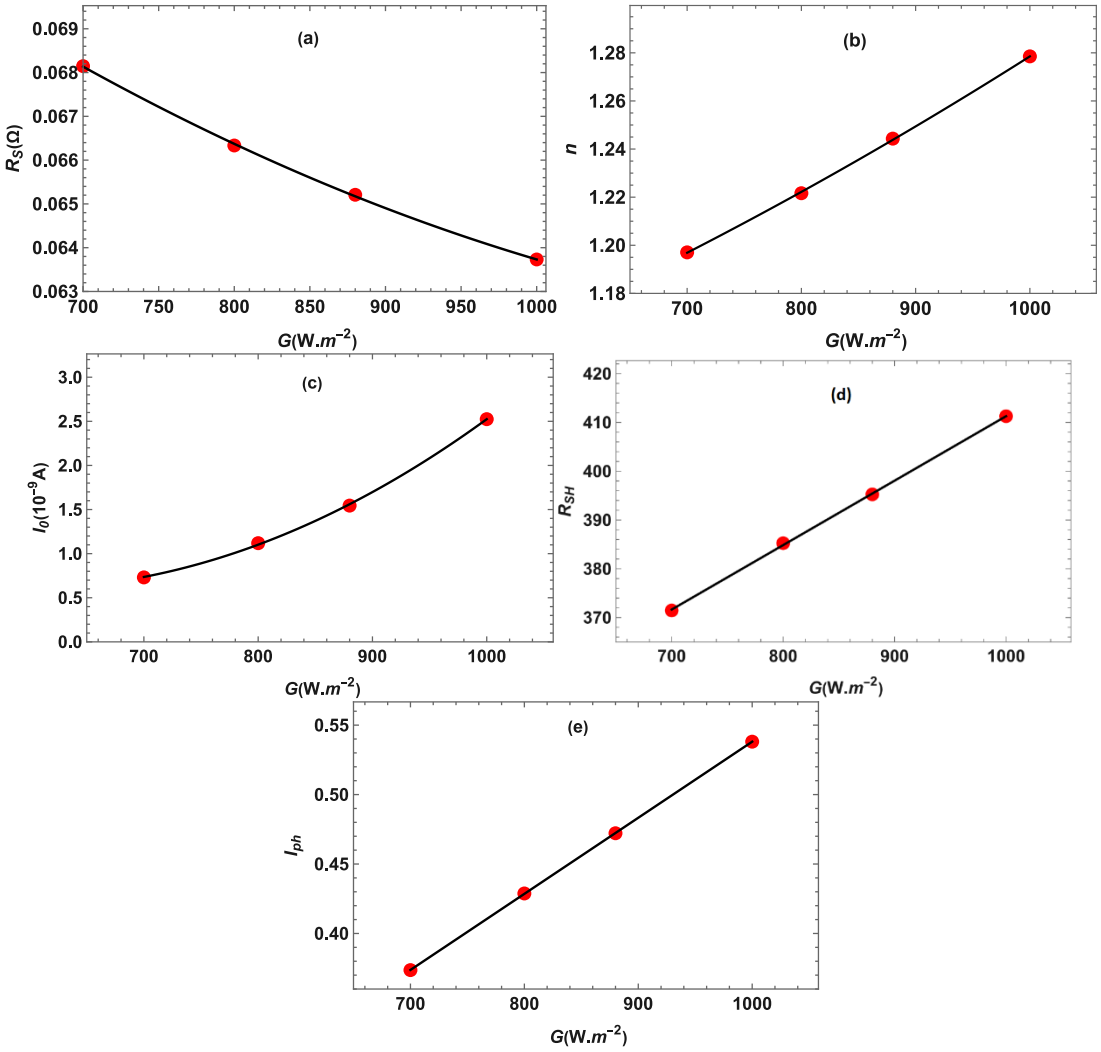

Figure. 8 PVG physical parameters (R_S, n, R_{SH}, I_0, I_{ph}) evolution as a function of irradiance for T_M = 25 °C: extracted values (•) and fitted curves obtained by linear regression (−)

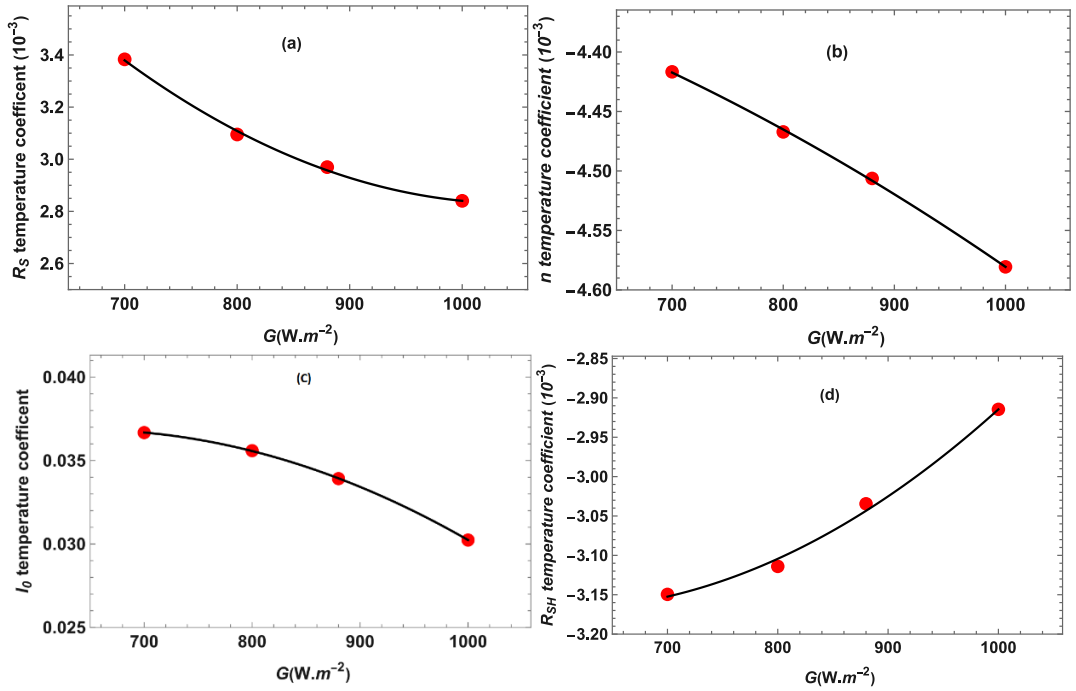

Figure. 9 G influence on temperature coefficients of n, I_0, R_S and R_{SH}, deduced from the fitting curves of Fig. 7

Table 5. Variation laws of PVG physical parameters with respect to T_M and G

Model	coefficient values	R^2	MARE
$R_S(T_M,G)=R_{S,ref}\left[1+coefT_{Rs}\left(T_M-T_{ref}\right)\right]\times\left[1+b_1\left(G-G_{ref}\right)+b_2\left(G-G_{ref}\right)^2\right]$ (12) Where : $coefT_{Rs}=a_1\left[1+a_2\left(G-G_{ref}\right)+a_3\left(G-G_{ref}\right)^2\right]$	$R_{S,ref}$ = 0.0637 Ω a_1 = 2.84×10^{-3} °C^{-1} a_2 = - 1.50×10^{-4} W^{-1}.m^2 a_3 = 1.61×10^{-6} W^{-2}.m^4 b_1 = - 1.61×10^{-4} W^{-1}.m^2 b_2 = 2.32×10^{-7} W^{-2}.m^4	*G = 1000 W.m^{-2}* *0.998* *G = 800 W.m^{-2}* *0.997*	*MARE* *8×10^{-4}* *6×10^{-3}*
$n(T_M,G)=n_{ref}\left[1+coefT_n\left(T_M-T_{ref}\right)\right]\times\left[1+b_3\left(G-G_{ref}\right)+b_4\left(G-G_{ref}\right)^2\right]$ (13) Where : $coefT_M=a_4\left[1+a_5\left(G-G_{ref}\right)+a_6\left(G-G_{ref}\right)^2\right]$	n_{ref} = 1.2785 a_4 = - 4.58×10^{-3} °C^{-1} a_5 = 1.40×10^{-4} W^{-1}.m^2 a_6 = 7.18×10^{-8} W^{-2}.m^4 b_3 = 2.35×10^{-4} W^{-1}.m^2 b_4 = 7.44×10^{-8} W^{-2}.m^4	*G = 1000 W.m^{-2}* *0.997* *G = 800 W.m^{-2}* *0.996*	*1×10^{-3}* *6×10^{-3}*
$I_0(T_M,G)=I_{0,ref}\left[1+b_5\left(G-G_{ref}\right)+b_6\left(G-G_{ref}\right)^2\right]Exp\left[coefT_{Io}\left(T_M-T_{ref}\right)\right]$ (14) Where: $coefT_M=a_7\left[1+a_8\left(G-G_{ref}\right)+a_9\left(G-G_{ref}\right)^2\right]$	$I_{0,ref}$ = 2.5×10^{-9} A a_7 = 0.0302 °C^{-1} a_8 = -1.22×10^{-3} W^{-1}.m^2 a_9 = -1.71×10^{-6} W^{-2}.m^4 b_5 = 3.73×10^{-3} W^{-1}.m^2 b_6 = 4.56×10^{-6} W^{-2}.m^4	*G = 1000 W.m^{-2}* *0.994* *G = 800 W.m^{-2}* *0.985*	*5×10^{-3}* *2×10^{-2}*
$R_{SH}(T_M,G)=R_{SH,ref}\left[1+coefT_{Rsh}\left(T_M-T_{ref}\right)\right]\times\left[1+b_7\left(G-G_{ref}\right)\right]$ (15) Where: $coefT_M=a_{10}\left[1+a_{11}\left(G-G_{ref}\right)+a_{12}\left(G-G_{ref}\right)^2\right]$	$R_{SH,ref}$ = 411 Ω a_{10} = - 2.91×10^{-3} °C^{-1} a_{11} = - 4.33×10^{-4} W^{-1}.m^2 a_{12} = - 5.36×10^{-7} W^{-2}.m^4 b_7 = 3.21×10^{-4} W^{-1}.m^2	*G = 1000 W.m^{-2}* *0.995* *G = 800 W.m^{-2}* *0.996*	*2×10^{-3}* *1.5×10^{-3}*
$I_{ph}(T_M,G)=I_{SC,ref}\times\frac{G}{G_{ref}}\left[1+coefT_{Iph}\left(T_M-T_{M,ref}\right)\right]$ (16)	$I_{SC,ref}$ = 0.5381 A $coefT_{Iph}\approx$ 0.0006 °C^{-1}	*G = 1000 W.m^{-2}* *0.998* *G = 800 W.m^{-2}* *0.990*	*2.5×10^{-5}* *3×10^{-3}*

results in the breaking of many atomic bonds by the released low energy, thus creating additional sites of recombination and enhancing the recombination effect [4]. In Fig. 8 (a), it is shown that, in the studied irradiance range from 700 to 1000W/m^2, at temperature of 25°C, the series resistance R_S decreases polynomially. This can be attributed to the conductivity improvement in the active layer owing to the photogenerated carriers increase [22].

4.4 Modeling of physical parameters changes depending on T_M and G

From regression analysis of the physical parameter variations with respect to T_M and G, Eq. (12) to Eq. (16) were derived (Table 5). The table includes also the values of temperature and irradiation coefficients, as well as physical parameters at reference state. These equations have the advantage of taking into account the G effect on the temperature coefficients by including specific terms.

In order to assess the reliability of the parameter behavior description by the proposed equations, we present the comparison results with some expressions commonly used in the literature (Eq. (17) to Eq. (36) and Fig. 10 to Fig. 15).

The prediction accuracy of the proposed equations is evaluated by comparison with some other commonly used in scientific literature. The T_M effect on I_0, n, R_S, and R_{SH} is assessed for G = 1000 W.m^{-2}.

- **Saturant current I_0 versus T_M [2]**

$$I_0=I_{0,ref}\left(\frac{T_M}{T_{ref}}\right)^{3/A}Exp\left(\frac{qE_{g,ref}}{Ak_B}\left(\frac{1}{T_{ref}}-\frac{1}{T_M}\right)\right) \quad (17)$$

$$I_0=I_{0,ref}\left(\frac{T_M}{T_{ref}}\right)^{3}Exp\left(\frac{qE_{g,ref}}{Ak_B}\left(\frac{1}{T_{ref}}-\frac{1}{T_M}\right)\right) \quad (18)$$

$$I_0=I_{0,ref}\left(\frac{T_M}{T_{ref}}\right)^{3}Exp\left(\frac{q}{Ak_B}\left(\frac{E_{g,ref}}{T_{ref}}-\frac{E_g}{T_M}\right)\right) \quad (19)$$

$$I_0=c_1{T_M}^3Exp\left(\frac{c_2}{T_M}\right) \quad (20)$$

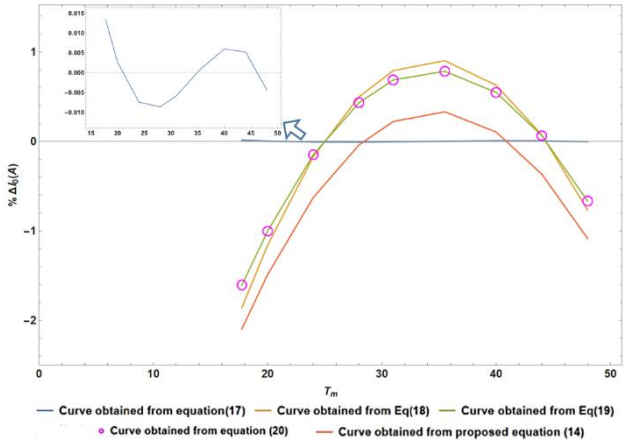

Figure. 10 Error rate between values of I_0 predicted using the models and I_0 extracted, for G= 1000 W.m^{-2}

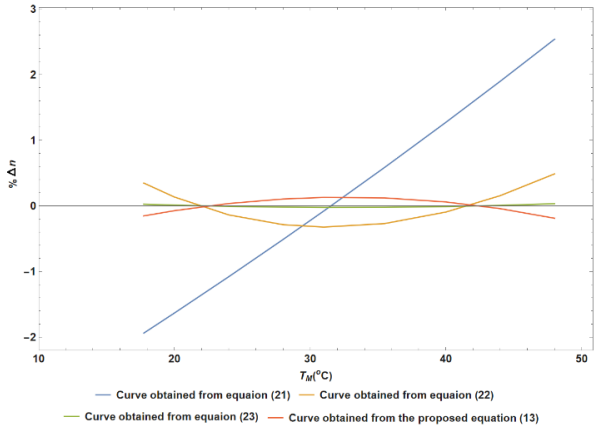

Figure. 11 Error rate between the values of n predicted usin the models and n extracted, for G= 1000 W.m^{-2}

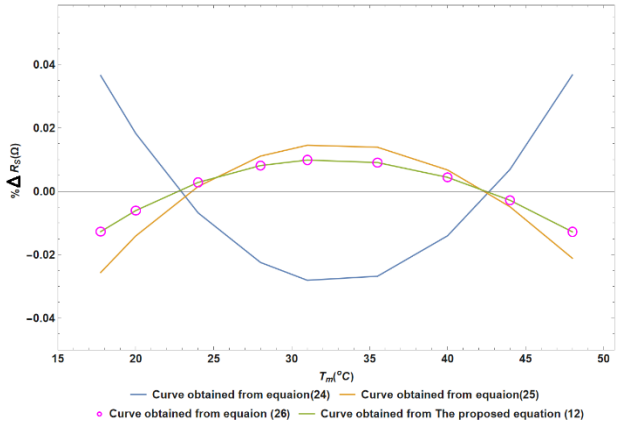

Figure. 12 Error rate between the values of R_S predicted using the models and R_S extracted, for G= 1000 W.m^{-2}

- **Ideality factor n versus T_M [23]**

$$n = c_3/T_M \tag{21}$$

$$n = \left(1 - c_4/{T_M}^2\right)^{-1} \tag{22}$$

$$n = 1 + c_5/T_M \tag{23}$$

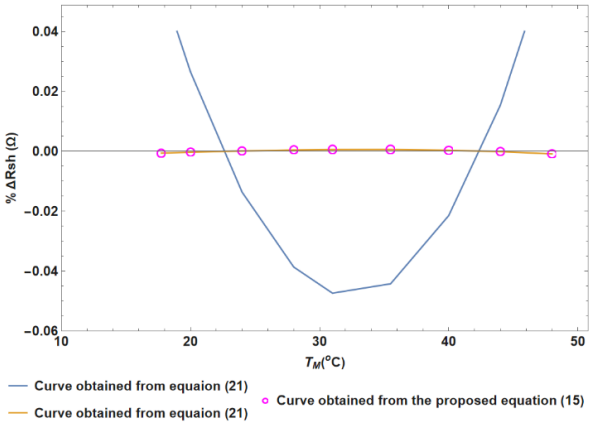

Figure. 13 Error rate between the values of R_{SH} predicted using the models and R_{SH} extracted, for G= 1000 W.m^{-2}

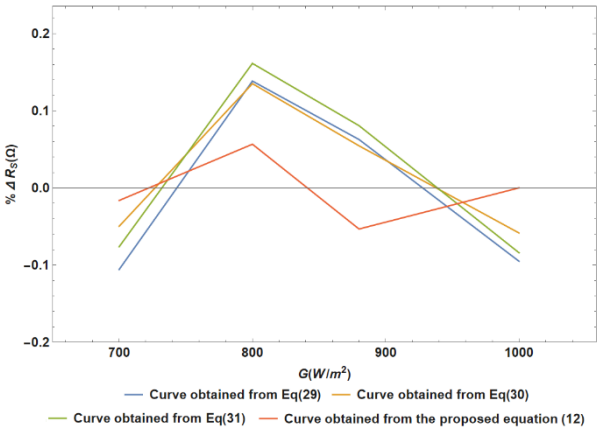

Figure. 14 Error rate between the values of R_S predicted using the models and R_S extracted, for T_M= 25ºC

- **Series resistance R_S versus T_M [24]–[26]**

$$R_S = R_{S,ref} Exp\left(c_6\left(T_M - T_{ref}\right)\right) \tag{24}$$

$$R_S = R_{S,ref}\left(T_M/T_{ref}\right)^{c_7} \tag{25}$$

$$R_S = c_7\left(T_M/T_{ref}\right) + c_8 \tag{26}$$

- **Shunt resistance R_{SH} versus T_M [1], [24]**

$$R_{SH} = c_9 Exp(c_{10}/T_M) \tag{27}$$

$$R_{SH} = R_{SH,ref}\left(1 + c_{11}\left(T_M - T_{ref}\right) + c_{12}\left(T_M - T_{ref}\right)^2\right) \tag{28}$$

The prediction accuracy of G effect on R_S, R_{SH}, and n is evaluated for a constant temperature T_M = 25 ºC.

- **Series resistance R_S versus G** [26– 28]

$$R_S = d_1\left(G/G_{ref}\right)^{d_2} \tag{29}$$

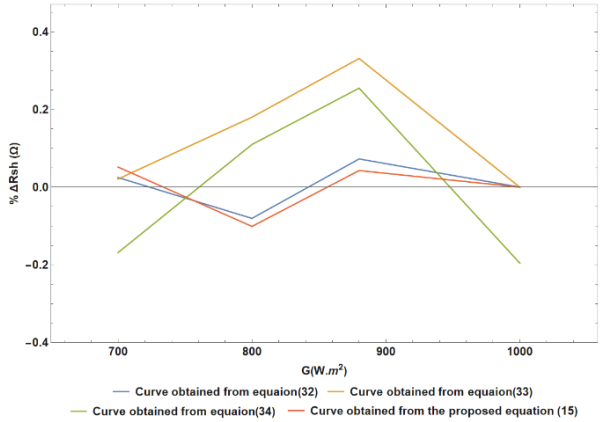

Figure. 15 Error rate between the values R_{SH} predicted using the models and R_{SH} extracted, for T_M= 25ºC

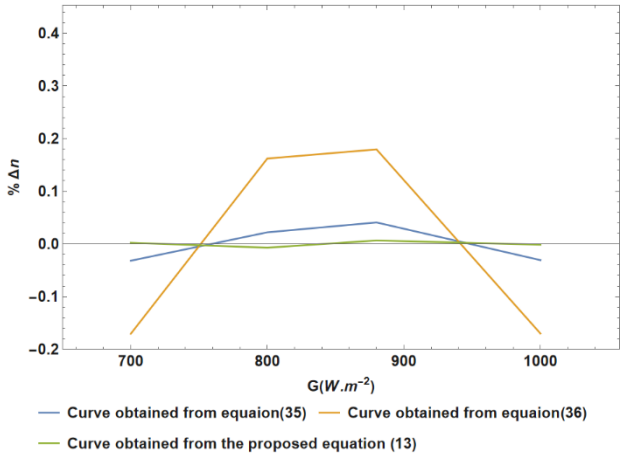

Figure. 16 Error rate between the values of n predicted using the models and those extracted, for T_M= 25ºC

$$R_S = d_3\left(1 - d_4 ln\left(G/G_{ref}\right)\right) \quad (30)$$

$$R_S = d_5\left(G/G_{ref}\right)^b + d_6 \quad (31)$$

- **Shunt resistance R_{SH} versus G [1]–[3]**

$$R_{SH} = d_7\left(G/G_{ref}\right) \quad (32)$$

$$R_{SH} = d_8\left(G/G_{ref}\right)^{d_9} \quad (33)$$

$$R_{SH} = d_{10} + d_{11}\, ln(G) \quad (34)$$

- **Ideality factor n versus G [3]**

$$n = d_{12} + d_{13}\, G \quad (35)$$

$$n = d_{14} + d_{15}\, ln(G) \quad (36)$$

Fig. 10 to Fig. 16 show a good compatibility of the proposed law with the experimental results presented, comparable with those presented in the scientific literature. The lower values of the error rate, obtained by the various laws, attest to the reliability of both the experimental data collected and the proposed equations.

In the scientific literature, empirical laws are reported where the influences of G and T_M on physical parameters appear decorrelated [2, 28]:

Table 6. Statistical evaluation of prediction using the proposed equation and Eq. (37)

G	Eq. (37) With : R_{ref2} = 0.0199 Ω, R_{ref2} = 0.0438Ω, c_{13} = 0.0045 and d_{16} = -0.549		Proposed Eq. (12)	
	R^2	MRAE	R^2	MRAE
1000	0.992	0.002	0.999	7×10^{-5}
890	0.899	$2{,}5\times10^{-3}$	0.990	2×10^{-3}
800	0.997	9×10^{-4}	0.998	6×10^{-5}
700	0.979	2×10^{-4}	0.997	7×10^{-4}

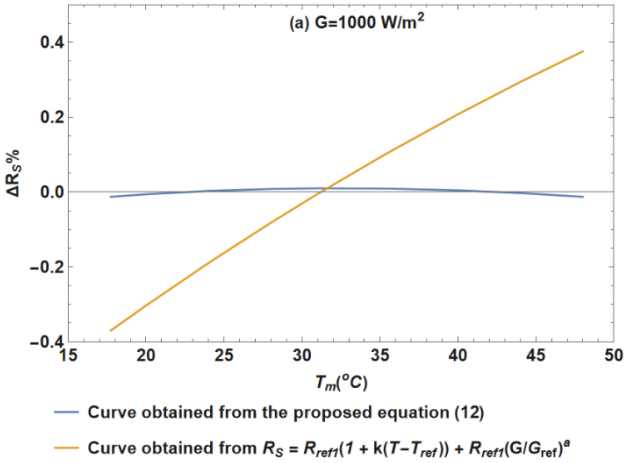

Figure. 17 Error rate between the *Rs* values predicted by the models and those extracted, obtained using proposed equation and Eq. (37) equations for G=1000 W.m^{-2}

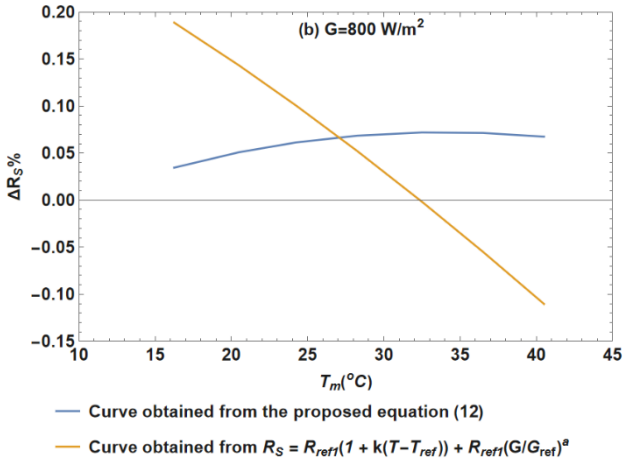

Figure. 18 Error rate between the *Rs* values predicted by the models and those extracted, obtained using proposed equation and Eq. (37) for G=800 W.m^{-2}

Table 7. Statistical evaluation of prediction using the proposed equation and Eq. (38)

G	Eq. (38) With : n_0 = 1.235, c_{14} = 0.0052, and d_{17} = 4.7×10^{-6}		Proposed Eq. (13)	
	R^2	MRAE	R^2	MRAE
1000	0.5565	0.0309	0.9994	10^{-5}
890	0.9698	0.0065	0.9976	0.0018
800	0.9111	0.0108	0.9995	6×10^{-4}
700	0.0180	0.0329	0.9980	0.0013

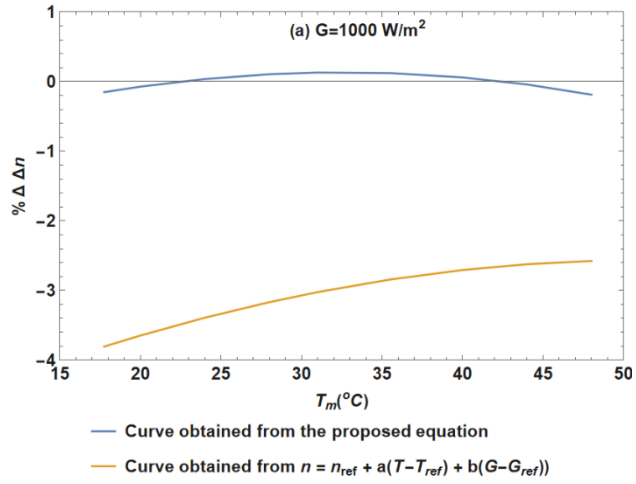

Figure. 19 Error rate between the *n* values predicted by the models and those extracted, obtained using proposed equation and Eq. (38) for G=1000 W.m^{-2}

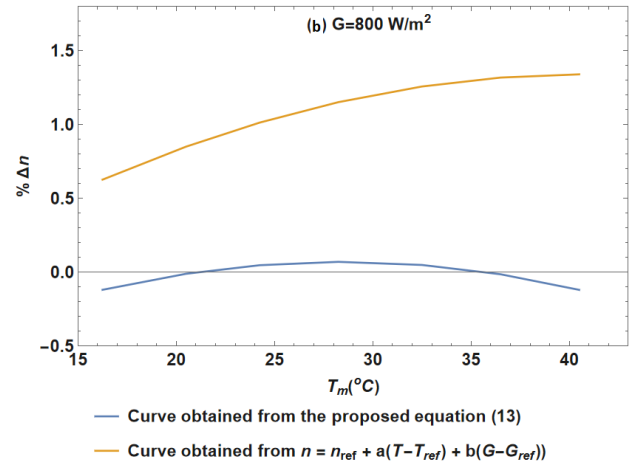

Figure. 20 Error rate between the *n* values predicted by the models and those extracted, obtained using proposed equation and Eq. (38) equations for *G*=800 m^{-2}

$$R_s = R_{ref2}\left(1 + c_{13}\left(T_M - T_{ref}\right)\right) + R_{ref1}\left(\frac{G}{G_{ref}}\right)^{d_{16}} \quad (37)$$

$$n = n_0 + c_{14}\left(T_M - T_{ref}\right) + d_{17}\left(G - G_{ref}\right) \quad (38)$$

By regression analysis we obtain the results presented in Tables 6 and 7 and Fig. 17 to Fig. 20.

Tables 6 and 7 and Fig. 16 to Fig. 20 show a best compatibility of the proposed laws given by Eq. (12) and Eq. (13) with the experimental results, compared to those given by Eq. (37) and Eq. (38). The values of the statistical indicators (R^2 and MARE) attest to the degrees of reliability of the two proposed equations. This highlights the importance of the proposed laws that combine the effects of G and T in a correlated way.

4.5 PV module performances prediction

The I-V characteristics as well as the output power of the PV modules for a given T_M and G can be determined using the equations presented in Table 5. To this end, Lambert's W function [17] was utilized to explicitly express the PVG module performance in terms of physical parameters and voltage (Eq. (39) to Eq. (42)).

$$I = \frac{V/(N_S R_{SH}) - I_0 - I_{ph}}{1 + R_S/R_{SH}} + \frac{n\,V_{th}}{R_S} \times W\left\{\frac{R_S.I_0}{n\,V_{th}(1+R_S/R_{SH})} exp\left(\frac{V/N_S + R_S(I_0+I_{ph})}{n\,V_{th}(1+R_S/R_{SH})}\right)\right\} \quad (39)$$

$$Power = V\left\{\frac{V/(N_S R_{SH}) - I_0 - I_{ph}}{1 + R_S/R_{SH}} + \frac{n\,V_{th}}{R_S} \times W\left\{\frac{R_S.I_0}{n\,V_{th}(1+R_S/R_{SH})} exp\left(\frac{V/N_S + R_S(I_0+I_{ph})}{n\,V_{th}(1+R_S/R_{SH})}\right)\right\}\right\} \quad (40)$$

$$I_{SC} = \frac{-I_0 - I_{ph}}{1 + R_S/R_{SH}} + \frac{n\,V_{th}}{R_S} \times W\left\{\frac{R_S.I_0}{n\,V_{th}(1+R_S/R_{SH})} exp\left(\frac{R_S(I_0+I_{ph})}{n\,V_{th}(1+R_S/R_{SH})}\right)\right\} \quad (41)$$

$$V_{OC} = N_S\left\{R_{SH}(I_0 + I_{ph}) + n\,V_{th} \times W\left\{\frac{R_{SH}.I_0}{n\,V_{th}} exp\left(\frac{R_{SH}(I_0+I_{ph})}{n\,V_{th}}\right)\right\}\right\} \quad (42)$$

Where, N_S stands for the number of cells in the module linked in series.

Using these equations together with the proposed Eq. (12) to Eq. (16), the performance of PV generators and their current-voltage characteristics can be predicted under real operating conditions (Fig. 21).

This technique can form a basis for forecasting the PV module performances and can be incorporated into maximum power point tracking (MPPT) programs to extract peak power output under different operating conditions. Indeed, PV modules exhibit non-linear *I-V* characteristics, with a maximum power point (MPP), which depends on temperature and irradiance (Fig. 10). In order to match the PV modules to the load, they

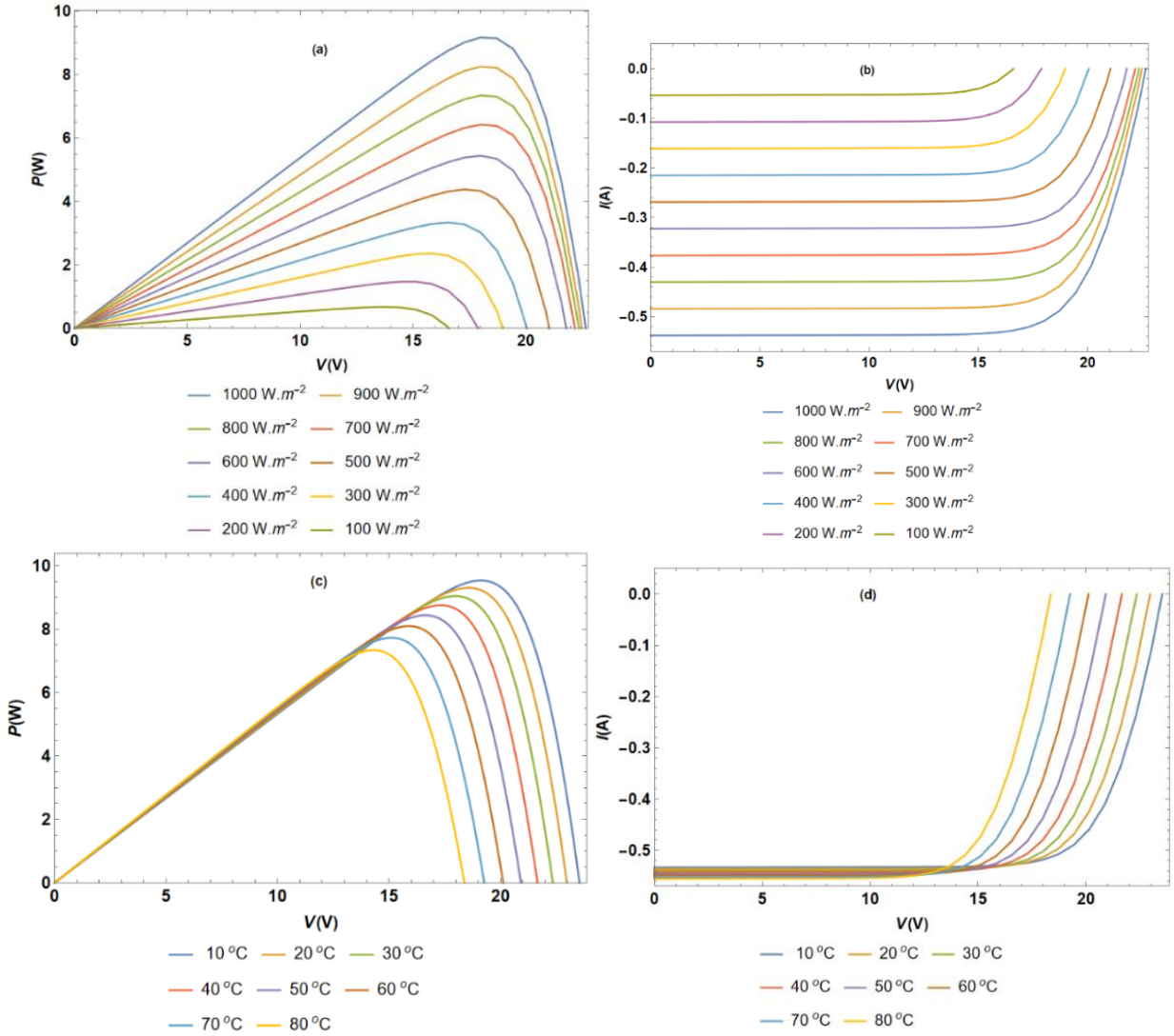

Figure. 21 Prediction of the power (a and c) and current-voltage characteristic (b and d) of the module under different operating temperature and irradiance conditions

must operate at their MPP despite the changes in weather conditions through the use of MPPT. When the weather parameters change, the new MPP must be found as soon as possible. Moreover, the automated systems used to find PPM must also ensure a good dynamic operation of the PV system. The most commonly used MPPT methods [29] are perturbation and observation (P&O), conductance increment (CI) and fractional open circuit voltage (FCO). They consist in measuring some electrical parameters generated by the PV generator using sensors, in order to monitor instantly the PPM. The P&O algorithm involves perturbing the PV module voltage around its initial value, and then analyzing the variation of the PV power output. The conductance increment (CI) algorithm, builds on the fact that the derivative of the PV module output power with respect to the voltage is zero at MPP. The FCO algorithm is based on the principle that the voltage at the maximum power point is always a constant fraction of V_{OC}. The open circuit voltage is measured and then used as an input for the monitor.

Reliability, accuracy and tracking speed are key factors in evaluating the performance of MPPT controls. For the three presented methods, it is difficult to reach simultaneously a fast-tracking time with high accuracy. This problem multiplies when there are sudden variations or the presence of partial shading that covers a fraction of the GPV. Injecting the proposed equations into the MPPT algorithms and using T_M and G measurement sensors can contribute to increase prediction efficiencies of MPP by simultaneously improving tracking speed and accuracy.

5 Conclusion

This work, aimed at predicting the PV modules performance from the physical parameter's behavior with respect to the G and T_M has led to the following

conclusions:

- The lower values of the error between experimentally extracted data and data predicted by means of the various scientific literature laws, attest to the reliability of the experimental data collected. This also reveals the importance of using regression equations to minimize the uncertainty in the evolution of the experimental data versus *T* and *G*.
- R_S, I_{ph}, *n* and R_{sh} vary linearly with T_M with a negative coefficient for R_S, I_{ph} and positive for the remaining two parameters. I_0 follows an exponential law and increases with T_M.
- R_S, *n* and I_0 vary polynomially with *G* with an increase of *n*, I_0 and a decrease of R_S as G increases. Both other parameters R_{sh} and I_{ph} grow linearly with G.
- The proposed laws, which combine the effects of *G* and *T* in a correlated way, allow to better predict the behavior of the physical parameters.
- The new proposed laws represent laws that, for the first time in the scientific literature, take into account the G effect on the temperature coefficients by including specific terms.
- The proposed laws can be used as a basis for forecasting the crystalline photovoltaic cells performance and to locate the maximum power point under changing climatic conditions.

Despite the better compatibility of the proposed laws with the experimental results presented in this work, it is recommended to confirm their reliability by conducting the study over wider temperature and irradiance ranges. For this purpose, this work will be extended to larger intervals of T_M and *G* values and will investigate the behavior of other PV module technologies such as polycrystalline and perovskite.

Conflicts of interest

The authors declare no conflict of interest.

Author contributions

Conceptualization, methodology, software, investigation validation, writing—original draft preparation, 1st, 2nd, 3rd, 4th, and 8th authors; formal analysis, 1st, 3rd, 5th, and 8th; resources and data curation and visualization, 5th, 6th, 7th and 8th authors; writing—review and editing, 2th, 3th, 4th, 6th, and 7th; supervision, 4th and 8th authors.

Nomenclature

PV	Photovoltaic
PVG	Photovoltaic generator
T	Temperature *[°C]*
T_M	Module temperature *[°C]*
T_{ref}	Reference temperature *[°C]*
G	Irradiance $[W/m^2]$
MPPT	Maximum Power Point Tracking
MPP	Maximum Power Point
I_{SC}	Short circuit current *[A]*
V_{OC}	Open circuit voltage *[V]*
I_m	Maximum power current *[A]*
V_m	Maximum power voltage *[V]*
I	Module terminal Current *[A]*
V	Module output voltage *[V]*
SDM	Single diode model
I_0	Reverse saturation current [*A]*
n	Ideality factor
I_{ph}	Photo-generated current *[A]*
R_S	Series resistance *[Ω]*
R_{SH}	Shunt resistance *[Ω]*
R_{S0}	Slope of the *I-V* characteristic at the short circuit point *[Ω]*
R_{SH0}	Slope of the *I-V* characteristic at the open circuit point *[Ω]*
V_{th}	Thermal voltage *[V]*
e	Electron charge $(=1{,}6.10^{-19}\ C)$
k_B	Boltzmann constant $(=1.3806\times10^{-23}\ J/K)$
STC	Standard test conditions ($T = 25$ °C, $G_0 = 1000\ W/m^2$ and $AM=1.5$)
N_S	PV module Cells number connected in series
P_m	Maximum power *[W]*
α_i	Temperature coefficient of PV module performance (i=1, 2, …)
β_i	Irradiance coefficient of PV module performance (i=1, 2, …)
$CoefT_i$	Temperature coefficients of the predicted physical parameters (I =R_S, R_{SH}, n, and I_0)
a_i	Coefficient of G influence on temperature coefficients of the predicted physical parameters (i=1, 2, …)
bi	Irradiance coefficients on predicted physical parameters (i=1, 2, …)
c_i	Physical parameters coefficient temperature of laws derived from literature (i=1, 2, …)
d_i	Physical parameters coefficient irradiance of laws derived from literature (i=1, 2, …)
$V_{m,\,ref}$	Maximum power voltage at reference

	state *[V]*
$T_{M,\,ref}$	Reference operating temperature (25°C)
$V_{OC,\,ref}$	Open circuit voltage at reference state *[V]*
$G_{ref,}$	Reference irradiation $[W/m^2]$
$I_{sc,\,ref}$	Short circuit current at reference state *[A]*
$I_{m,\,,ref}$	Maximum power current at reference state *[A]*
$I_{0,\,ref}$	Saturation current at reference state *[A]*
n_{ref}	Ideality factor at reference state
$R_{S,\,ref}$	Series resistance at reference state *[Ω]*
$R_{SH,\,ref}$	shunt resistance at reference state *[Ω]*
MARE	Mean Absolute Relative Error
R^2	Coefficient of determination
erMax	Maximum absolute relative error
I_{avg}	Average value of the measured current
$I_{,mi}$	i^{th} measured current intensity.
I_{ci}	i^{th} extracted current intensity;
p	number of points that have been measured experimentally

References

[1] S. Yadir, R. Bendaoud, A. E. Abidi, H. Amiry, M. Benhmida, S. Bounouar, B. Zohal, H. Bousseta, A. Zrhaiba, and A. Elhassnaoui, "Evolution of the physical parameters of photovoltaic generators as a function of temperature and irradiance: New method of prediction based on the manufacturer's datasheet", *Energy Conversion and Management*, Vol. 203, p. 112141, 2020, doi: 10.1016/j.enconman.2019.112141.

[2] R. Bendaoud, H. Amiry, M. Benhmida, B. Zohal, S. Yadir, S. Bounouar, C. Hajjaj, E. Baghaz, and M. E. Aydi, "New method for extracting physical parameters of PV generators combining an implemented genetic algorithm and the simulated annealing algorithm", *Solar Energy*, Vol. 194, pp. 239–247, 2019, doi: 10.1016/j.solener.2019.10.040.

[3] D. R. Ahmed, H. M. Abdullah, and F. F. Muhammadsharif, "Utilization of device parameters to assess the performance of a monocrystalline solar module under varied temperature and irradiance", *Energy Syst*, 2021, doi: 10.1007/s12667-021-00472-6.

[4] M. Chegaar, A. Hamzaoui, A. Namoda, P. Petit, M. Aillerie, and A. Herguth, "Effect of Illumination Intensity on Solar Cells Parameters", *Energy Procedia*, Vol. 36, pp. 722–729, 2013, doi: 10.1016/j.egypro.2013.07.084.

[5] F. Khan, S. N. Singh, and M. Husain, "Effect of illumination intensity on cell parameters of a silicon solar cell", *Solar Energy Materials and Solar Cells*, Vol. 94, No. 9, pp. 1473–1476, 2010, doi: 10.1016/j.solmat.2010.03.018.

[6] L. H. I. Lim, Z. Ye, J. Ye, D. Yang, and H. Du, "A linear method to extract diode model parameters of solar panels from a single I–V curve", *Renewable Energy*, Vol. 76, pp. 135–142, 2015, doi: 10.1016/j.renene.2014.11.018.

[7] A. M. Humada, M. Hojabri, S. Mekhilef, and H. M. Hamada, "Solar cell parameters extraction based on single and double-diode models: A review", *Renewable and Sustainable Energy Reviews*, Vol. 56, pp. 494–509, 2016, doi: 10.1016/j.rser.2015.11.051.

[8] D. M. Fébba, R. M. Rubinger, A. F. Oliveira, and E. C. Bortoni, "Impacts of temperature and irradiance on polycrystalline silicon solar cells parameters", *Solar Energy*, Vol. 174, pp. 628–639, 2018, doi: 10.1016/j.solener.2018.09.051.

[9] P. Singh, S. Singh, M. Lal, and M. Husain, "Temperature dependence of I–V characteristics and performance parameters of silicon solar cell", *Solar Energy Materials and Solar Cells*, Vol. 92, No. 12, pp. 1611–1616, 2008, doi: 10.1016/j.solmat.2008.07.010.

[10] M. Wang, J. Peng, Y. Luo, Z. Shen, and H. Yang, "Comparison of different simplistic prediction models for forecasting PV power output: Assessment with experimental measurements", *Energy*, Vol. 224, p. 120162, 2021, doi: 10.1016/j.energy.2021.120162.

[11] J. Peng, L. Lu, H. Yang, and T. Ma, "Validation of the Sandia model with indoor and outdoor measurements for semi-transparent amorphous silicon PV modules", *Renewable Energy*, Vol. 80, pp. 316–323, 2015, doi: 10.1016/j.renene.2015.02.017.

[12] I. D. L. Parra, M. Muñoz, E. Lorenzo, M. García, J. Marcos, and F. M. Moreno, "PV performance modelling: A review in the light of quality assurance for large PV plants", *Renewable and Sustainable Energy Reviews*, Vol. 78, pp. 780–797, 2017, doi: 10.1016/j.rser.2017.04.080.

[13] M. Zaimi, H. E. Achouby, O. Zegoudi, A. Ibral, and E. M. Assaid, "Numerical method and new analytical models for determining temporal changes of model-parameters to predict maximum power and efficiency of PV module operating outdoor under arbitrary conditions", *Energy Conversion and Management*, Vol. 220,

p. 113071, 2020, doi: 10.1016/j.enconman.2020.113071.

[14] M. Adar, M. A. Babay, S. Touairi, Y. Najih, and M. Mabrouki, "Experimental validation of different PV power prediction models under Beni Mellal climate, implications for the energy nexus", *Energy Nexus*, Vol. 5, p. 100050, 2022, doi: 10.1016/j.nexus.2022.100050.

[15] J. Peng, L. Lu, H. Yang, and T. Ma, "Validation of the Sandia model with indoor and outdoor measurements for semi-transparent amorphous silicon PV modules", *Renewable Energy*, Vol. 80, pp. 316–323, 2015, doi: 10.1016/j.renene.2015.02.017.

[16] M. Zaimi, H. E. Achouby, O. Zegoudi, A. Ibral, and E. M. Assaid, "Numerical method and new analytical models for determining temporal changes of model-parameters to predict maximum power and efficiency of PV module operating outdoor under arbitrary conditions", *Energy Conversion and Management*, Vol. 220, p. 113071, 2020, doi: 10.1016/j.enconman.2020.113071.

[17] S. Yadir, M. Benhmida, M. Sidki, E. Assaid, and M. Khaidar, "New method for extracting the model physical parameters of solar cells using explicit analytic solutions of current-voltage equation", in *2009 International Conference on Microelectronics - ICM*, Marrakech, Morocco, pp. 390–393, 2009. doi: 10.1109/ICM.2009.5418599.

[18] A. D. Dhass, P. Lakshmi, and E. Natarajan, "Investigation of Performance Parameters of Different Photovoltaic Cell Materials using the Lambert-W Function", *Energy Procedia*, Vol. 90, pp. 566–573, 2016, doi: 10.1016/j.egypro.2016.11.225.

[19] H. Tian, F. M. David, K. Ellis, E. Muljadi, and P. Jenkins, "A cell-to-module-to-array detailed model for photovoltaic panels", *Solar Energy*, Vol. 86, No. 9, pp. 2695–2706, 2012, doi: 10.1016/j.solener.2012.06.004.

[20] P. Singh and N. M. Ravindra, "Temperature dependence of solar cell performance—an analysis", *Solar Energy Materials and Solar Cells*, Vol. 101, pp. 36–45, 2012, doi: 10.1016/j.solmat.2012.02.019.

[21] P. Singh and N. M. Ravindra, "Temperature dependence of solar cell performance—an analysis", *Solar Energy Materials and Solar Cells*, Vol. 101, pp. 36–45, 2012, doi: 10.1016/j.solmat.2012.02.019.

[22] E. Cuce, P. M. Cuce, and T. Bali, "An experimental analysis of illumination intensity and temperature dependency of photovoltaic cell parameters", *Applied Energy*, Vol. 111, pp. 374–382, 2013, doi: 10.1016/j.apenergy.2013.05.025.

[23] J. Verschraegen, M. Burgelman, and J. Penndorf, "Temperature dependence of the diode ideality factor in CuInS2-on-Cu-tape solar cells", *Thin Solid Films*, Vol. 480–481, pp. 307–311, 2005, doi: 10.1016/j.tsf.2004.11.006.

[24] S. Bensalem and M. Chegaar, "Thermal behavior of parasitic resistances of polycrystalline silicon solar cells", *Revue des Energies Renouvelables*, Vol. 16, No. 1, pp. 171–176, 2013.

[25] W. T. da Costa, J. F. Fardin, D. S. L. Simonetti, and L. D. V. B. M. Neto, "Identification of photovoltaic model parameters by Differential Evolution", In: *Proc. of 2010 IEEE International Conference on Industrial Technology*, Vi a del Mar, Chile, pp. 931–936, 2010. doi: 10.1109/ICIT.2010.5472557.

[26] H. Ibrahim and N. Anani, "Variations of PV module parameters with irradiance and temperature", *Energy Procedia*, Vol. 134, pp. 276–285, 2017, doi: 10.1016/j.egypro.2017.09.617.

[27] C. S. Ruschel, F. P. Gasparin, and A. Krenzinger, "Experimental analysis of the single diode model parameters dependence on irradiance and temperature", *Solar Energy*, Vol. 217, pp. 134–144, 2021, doi: 10.1016/j.solener.2021.01.067.

[28] E. A. Silva, F. Bradaschia, M. C. Cavalcanti, A. J. Nascimento, L. Michels, and L. P. Pietta, "An Eight-Parameter Adaptive Model for the Single Diode Equivalent Circuit Based on the Photovoltaic Module's Physics", *IEEE J. Photovoltaics*, Vol. 7, No. 4, pp. 1115–1123, Jul. 2017, doi: 10.1109/JPHOTOV.2017.2703778.

[29] A. O. Baba, G. Liu, and X. Chen, "Classification and Evaluation Review of Maximum Power Point Tracking Methods", *Sustainable Futures*, Vol. 2, p. 100020, 2020, doi: 10.1016/j.sftr.2020.100020.